Bull Math Biol (2012) 74:958–980
DOI 10.1007/s11538-011-9704-y

ORIGINAL ARTICLE

Modeling Optimal Age-Specific Vaccination Strategies Against Pandemic Influenza

Sunmi Lee · Michael Golinski · Gerardo Chowell

Received: 12 August 2010 / Accepted: 28 October 2011 / Published online: 7 December 2011

Abstract In the context of pandemic influenza, the prompt and effective implementation of control measures is of great concern for public health officials around the world. In particular, the role of vaccination should be considered as part of any pandemic preparedness plan. The timely production and efficient distribution of pandemic influenza vaccines are important factors to consider in mitigating the morbidity and mortality impact of an influenza pandemic, particularly for those individuals at highest risk of developing severe disease. In this paper, we use a mathematical model that incorporates age-structured transmission dynamics of influenza to evaluate optimal vaccination strategies in the epidemiological context of the Spring 2009 A (H1N1) pandemic in Mexico. We extend previous work on age-specific vaccination strategies to time-dependent optimal vaccination policies by solving an optimal control problem with the aim of minimizing the number of infected individuals over the course of a single pandemic wave. Optimal vaccination policies are computed and analyzed under different vaccination coverages (21%–77%) and different transmissibility levels ($\mathcal{R}_0$ in the range of 1.8–3). The results suggest that the optimal vaccination can be achieved by allocating most vaccines to young adults (20–39 yr) followed by school age children (6–12 yr) when the vaccination coverage does not exceed 30%. For higher $\mathcal{R}_0$ levels ($\mathcal{R}_0 >= 2.4$), or a time delay in the implementation of vaccination (>90 days), a quick and substantial decrease in the pool of susceptibles would require the implementation of an intensive vaccination protocol within a shorter period of time. Our results indicate that optimal age-specific vaccination rates are significantly associated with $\mathcal{R}_0$, the amount of vaccines available and the timing of vaccination.

Keywords Influenza pandemic · A/H1N1 pandemic · Optimal control · Age-specific vaccination

S. Lee (✉) · M. Golinski · G. Chowell
Mathematical and Computational Modeling Sciences Center, School of Human Evolution and Social Change, Arizona State University, Tempe, AZ 85282, USA
e-mail: mathever@gmail.com

1 Introduction

The emergence of the highly transmissible novel influenza virus A (H1N1) among humans in Spring 2009 raised concerns about the potential morbidity and mortality impact of the pandemic virus worldwide. The development of optimal countermeasures is critical particularly when resources to reduce the severity of the pandemic are limited. This is relevant given the fact that existing production technologies cannot keep pace with the vaccination needs of an entire nation at the onset of a pandemic. The intensity of interventions required to mitigate an unfolding influenza pandemic is further complicated by substantial uncertainty levels associated with the epidemiology of pandemic influenza (e.g., transmissibility ($\mathcal{R}_0$) and case fatality rates), which calls for the development of systematic approaches for the generation of optimal control strategies. The timely and sufficient production of vaccine supplies is challenging, due to the fact that production against an emergent A (H1N1) influenza pandemic can only start once the pandemic virus has been identified. Therefore, current pandemic vaccine constraints inevitably lead to limited vaccine stockpiles that require effective prioritization schemes in the population (Oshitani et al. 2008). The implementation of national and global pandemic mitigation plans has been evaluated using a number of models (Chowell et al. 2008; Ferguson et al. 2006; Germann et al. 2006; Hill and Longini 2003; Lipsitch et al. 2009; Merler et al. 2009; Nishiura et al. 2009). For example, age-structured models have been developed to investigate the effects of optimization of vaccination allocations against pandemic influenza in terms of reducing the morbidity and mortality impact (Chowell et al. 2009; Knipl and Rost 2011; Mylius et al. 2008; Patel et al. 2005; Tuite et al. 2010). For instance, Medlock et al. (2009) determined optimal vaccine allocation for five outcome measures: deaths, infections, years of life lost, contingent evaluation, and economic costs. These types of studies, which are based on optimization methods, indicate that optimal vaccine allocations differ markedly for seasonal and pandemic influenza as they are dependent on the distribution of age and/or risk groups within a population.

The novel influenza A (H1N1) virus first generated significant impact in Mexico in April 2009. Early epidemiological pandemic data from Mexico indicated a substantial increase in morbidity and mortality rates among young adults compared to morbidity and mortality rates which are concentrated among the young and old during interpandemic influenza years (Chowell et al. 2009). Earlier work on pandemic vaccination strategies employed an age-structured model that was previously calibrated against local demographic and epidemiological data from the early wave of the 2009 influenza pandemic in Mexico (Chowell et al. 2009) to evaluate the impact of adaptive vaccination strategies. The adaptive vaccination strategies studied by Chowell et al. (2009) were shown to outperform seasonal influenza vaccination strategies. Here, we use the mathematical model (Chowell et al. 2009) as a basis to assess time variations in age-specific vaccination rates by incorporating time-dependent vaccination rates as optimal control functions. We used a novel model based on optimal control theory to determine age-specific vaccination allocation during pandemics. Our mathematical model was then used to answer questions germane to the effectiveness of optimal vaccination strategies including: (1) Which age groups should be prioritized for influenza pandemic vaccination? (2) How much vaccine should be allocated to

each group and how do these vaccination rates vary over time? We addressed these questions by formulating an optimal control problem with the goal of minimizing the number of infected individuals while minimizing cost of implementing vaccination over the duration of the pandemic. We also explored the impact of optimal age-specific vaccination strategies on the temporal dynamics of infection, hospitalization, and death under different vaccination coverage and epidemiological scenarios.

2 Influenza Pandemic Model with Time-Dependent Vaccination

Optimal control theory (Fleming and Rishel 1975; Pontryagin et al. 1962) has been used by a number of biological and epidemiological models (Blayneh et al. 2009; Jung et al. 2002; Lenhart and Workman 2007; Rowthorn et al. 2009). Recently, SIR models have incorporated vaccination, quarantine, and isolation controls (Behncke 2000; Hansen and Day 2010; Lee et al. 2011; Lenhart and Workman 2007; Rowthorn et al. 2009) to study the impact of optimal control on the spread of disease. For example, optimal antiviral treatment and isolation strategies have been evaluated in the context of the 1918 influenza pandemic (Lee et al. 2010). A constrained optimal control problem was solved to discuss optimal vaccination strategies for the 1918 influenza pandemic when vaccine supply is limited (Lee et al. 2011). In this paper, we formulated an optimal control problem in the context of the transmission dynamics of the 2009 influenza pandemic in Mexico that captures age-specific characteristics of the population (Chowell et al. 2009). The baseline model (Chowell et al. 2009) is modified through the incorporation of time-dependent (six age-specific) control functions $u_i(t)$, where $i = 1, \ldots, 6$. We employed time-dependent (age-specific) control functions to measure the effectiveness of age-specific vaccination policies aimed at minimizing the number of infected individuals during the pandemic. The dynamic model with age-specific controls is described by the following system of nonlinear differential equations:

$$
\begin{aligned}
\dot{S}_i(t) &= -u_i(t)S_i(t) - \sum_{i=1}^{6} \beta_{ij} \frac{(I_j(t) + J_j(t))}{N(t)} S_i(t) \\
\dot{V}_i(t) &= \epsilon_i u_i(t)S_i(t) - \eta V_i(t) - \sum_{i=1}^{6} \beta_{ij} \frac{(I_j(t) + J_j(t))}{N(t)} V_i(t) \\
\dot{F}_i(t) &= (1-\epsilon_i)u_i(t)S_i(t) - \sum_{i=1}^{6} \beta_{ij} \frac{(I_j(t) + J_j(t))}{N(t)} F_i(t) \\
\dot{P}_i(t) &= \eta V_i(t) \\
\dot{E}_i(t) &= \sum_{i=1}^{6} \beta_{ij} \frac{(I_j(t) + J_j(t))}{N(t)} \big(S_i(t) + V_i(t) + F_i(t)\big) - kE_i(t) \\
\dot{I}_i(t) &= kE_i(t) - (\alpha_i + \gamma_1)I_i(t) \\
\dot{J}_i(t) &= \alpha_i I_i(t) - (\gamma_2 + \delta_i)J_i(t) \\
\dot{R}_i(t) &= \gamma_1 I_i(t) + \gamma_2 J_i(t) \\
\dot{D}_i(t) &= \delta_i J_i(t)
\end{aligned}
\tag{1}
$$

The model classifies individuals as susceptible (S_i), effectively vaccinated but not yet protected (V_i), ineffectively vaccinated (F_i), protected by vaccination (P_i), latent (E_i), infectious in the population (I_i), hospitalized (J_i), recovered (R_i), and dead (D_i) for $i = 1, \ldots, 6$ (six age groups: 0–5 yr, 6–12 yr, 13–19 yr, 20–39 yr, 40–59 yr, >=60 yr). Susceptible individuals in age group i are exposed to the influenza virus at the force of infection $\sum_{i=1}^{6} \beta_{ij}(I_j(t) + J_j(t))/N(t)$ where β_{ij} is the transmission rate between age groups i and j. The total population size is given by $N(t) = \sum_{i=1}^{6} S_i(t) + V_i(t) + F_i(t) + P_i(t) + E_i(t) + I_i(t) + J_i(t) + R_i(t)$. The transmission rates β_{ij} are given by qc_{ij} where q is the transmission probability per contact (fraction of contacts that leads to infection), which is assumed to be constant across age groups and is adjusted to achieve the desired $\mathcal{R}_0$. The contact rate matrix, c_{ij} represents the mixing rates between age groups i and j with higher rates within each age group (when $i = j$) than between age groups when $i \neq j$ (see Fig. 1 and (9) in Appendix and more details are in Wallinga et al. 2006). Latent individuals E_i progress to the infectious class I_i at the rate k (where $1/k$ is the mean latent period). Infectious individuals are hospitalized at the age-specific mean rates α_i and recover at the mean rate γ_1. Hospitalized individuals either recover at the constant rate γ_2 or die from influenza at the age-specific rate δ_i. Age-specific rates for hospitalization and mortality are given in Fig. 1 and Table 2 (see also Chowell et al. 2009). Recovered individuals are assumed to remain protected for the duration of the pandemic. The control functions $u_i(t)$ determine the age-specific vaccination rates of susceptible individuals (S_i) *per unit of time* for each age group i. We assume that $V_i(t)$ achieve maximal per-capita vaccination rates $\epsilon_i u_i(t)$ with age-specific vaccine efficacy ϵ_i (Fig. 1 and Table 2). Vaccinated individuals are assumed to progress to the protected class P_i at the rate η (with mean $1/\eta = 10$ days) while the ineffectively vaccinated class F_i remain susceptible to infection. In addition, the vaccinated but not yet protected classes V_i are susceptible to infection.

The goal is to minimize the number of infectious individuals at a minimal cost via vaccination during the course of a single influenza pandemic outbreak $[0, T]$. The objective functional $\mathcal{F}$ to be minimized is given by the expression:

$$\mathcal{F}\big(U(t)\big) = \int_0^T \sum_{i=1}^{6} \left[I_i(t) + \frac{W_i}{2} {u_i}^2(t) \right] dt \tag{2}$$

with $U(t) = (u_1(t), \ldots, u_6(t))$ and $X(t) = (S_i, V_i, F_i, P_i, E_i, I_i, J_i, R_i, D_i)$. The age-dependent optimal vaccination strategies can be obtained by finding an optimal pair of solutions $(U^*(t), X^*(t))$ such that

$$\mathcal{F}\big(U^*(t)\big) = \min_{\Omega} \mathcal{F}\big(U(t)\big) \tag{3}$$

where $\Omega = \{U(t) \in L^2(0, T)^6 \| a \leq u_i(t) \leq b, i = 1, \ldots, 6, t \in [0, T]\}$ subject to the state equations given by (1). We assume that the control efforts are nonlinear (quadratic) to the objective functional and this can be generalized by using a combination of linear and quadratic functions of controls (but we only consider quadratic control functions in this work). Also, we assume that each age-specific control function $u_i(t)$ (age-specific vaccination rate) is bounded by the same constant a and b. The age-specific weight constants $W_i \geq 0$ represent the desired balancing constants

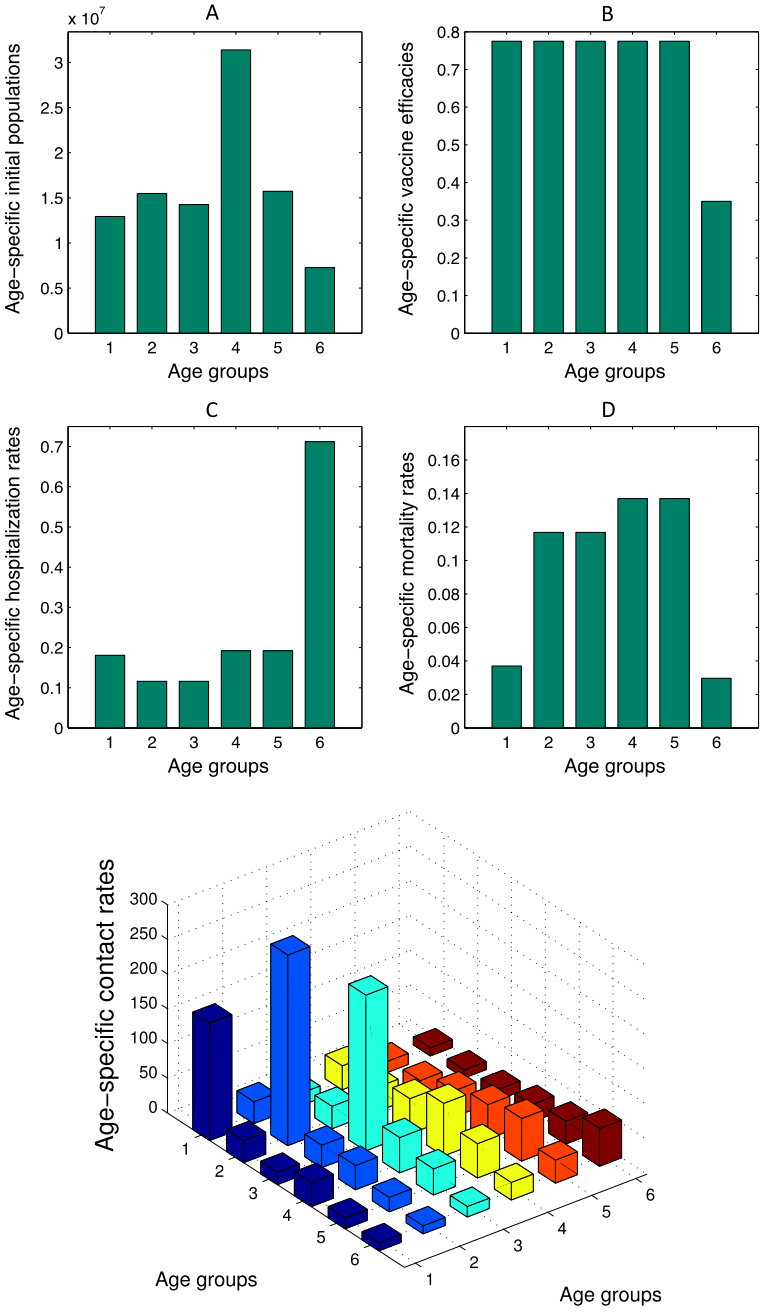

Fig. 1 The model consists of 6 age groups (1 = 0–5 yr, 2 = 6–12 yr, 3 = 13–19 yr, 4 = 20–39 yr, 5 = 40–59 yr, 6 = >60 yr). Age-dependent parameters (calibrated for the 2009 A (H1N1) outbreak in Mexico) are shown; population sizes, vaccine efficacies, hospitalization rates, and mortality rates (**A**)–(**D**). The age-specific contact rate matrix c_{ij} between age groups i and j per week is illustrated in the bottom panel. The contact rate among the 6–12 yr age group is the highest while it is lowest among seniors (=>60 yr)

which measure the relative cost of vaccination over a finite time period; for simplicity, that age-specific weight constants are assumed to be invariant across age groups as a baseline. This assumption can be further complicated by the relative costs among different age groups. Here, we adjust these relative costs for corresponding vaccination controls to limit a prespecified vaccination coverage indirectly. For example, a larger value of the weight constant lead to a smaller value of control (or vaccine) functions and this results in smaller vaccine coverage. Pontryagin's Maximum Principle (Lee et al. 2010; Lenhart and Workman 2007) is used to solve this optimal control problem and its optimality system is given in the Appendix.

3 Simulation Results

We present simulation results generated by the numerical implementation of optimal age-specific vaccination strategies as described in Sect. 2. First, we explore a baseline pandemic scenario in the context of the 2009 A (H1N1) outbreak in Mexico in the absence of vaccination. We evaluate the impact of optimal vaccination strategies on the dynamics of influenza pandemics under different vaccination coverages and different transmissibility levels. The estimated range of $\mathcal{R}_0$ for the 2009 influenza pandemic is around 1.6–3.0 (Chowell et al. 2009).

In our optimal control formulation, there are two critical parameter values (weight constants and a control upper bound), which associate with vaccination coverage and the maximum daily vaccination rate, respectively. In general, vaccination coverage for a pandemic influenza is much lower than 100% due to a lack of a vaccine at the onset of pandemic influenza. Especially, for 2009 H1N1 pandemic influenza, developed countries like the US or Canada achieved 30–40% vaccine coverage (Public Health Agency of Canada; CDC; Health Industry Distributors Association 2009; Macroepidemiology of Influenza Vaccination Study Group 2005; Oliver Wyman Group and Program for Appropriate Technology 2007) while developed countries including Mexico did not exceed 10–20% (Herrera-Valdez et al. 2011; Libenson 2009; Valadez 2010). Therefore, the weight constant has to be determined so that the total vaccination coverage lies in a realistic range. First, we varied weight constants in the $[1–10^{15}]$ range, which is chosen due to a large difference between the two terms in the objective functional (approximately 10^6–10^{10} between the number of infected individuals and the values of control functions). Then we explored the impact of the weight constants on the vaccination coverage. Extensive numerical experiments indicated weight constants in the range of $[1–10^6]$ resulting in a vaccine coverage of more than 80% of the total population, which is beyond realistic vaccination coverage levels. Finally, the weight constants are chosen in the range of 10^9–10^{15} ($W_i \in [10^9, 10^{15}]$ for $i = 1, \ldots, 6$).

The second major control parameter value is the control upper bound, which represents the maximum daily vaccination rate or the maximum daily rate of vaccine administration. There has been work to estimate the daily rate of vaccine administration and it is below 2% of the total population (Aaby et al. 2006; Centers For Disease Control and Prevention 2009; Cho et al. 2011; Peterborough County-City Health Unit Pandemic Influenza Plan 2010; Phillips and Williamson 2005; Tennenbaum 2008;

Table 1 Parameter definitions and baseline values (and their corresponding sources) used in numerical simulations. Parameter values were based on Chowell et al. 2009.

Parameter	Description	Value
k	Rate of progression from latent to infectious (days^{-1})	1/1.9
γ_1	Recovery rate (days^{-1}) for infectious class (days^{-1})	1/1.5
γ_2	Recovery rate for hospitalized class (days^{-1})	1/1.5
η	Rate of progression from vaccinated to protected (days^{-1})	1/10
α_i	Age-specific diagnostic rate (days^{-1})	0.12–0.7
δ_i	Age-specific mortality rate (days^{-1})	0.03–0.14
ϵ_i	Age-specific efficacy of vaccinations (%)	35–77
$I_i(0)$	The initial values ($i = 2, 3$)	1, 5
T	The simulated duration (days)	300
b	The upper bound of control (vaccination rates, days^{-1})	0.02
W_i	Weight constants on controls	10^9–10^{15}

Washington 2009). Since this is the estimation for developed countries, it is reasonable to assume 2% of the total population to be the maximum daily vaccination rate for developing countries like Mexico. Therefore, based on these findings, we must take this bound for control ($b = 0.02$ in (3)) to be realistic.

For model (1), the key parameters which determine the dynamics of the influenza pandemic include the age distribution of the population as well as age-specific vaccine efficacy, hospitalization rates, mortality rates, and contact rates (see Fig. 1 and Table 2). Vaccine efficacy is assumed to be 77.5% for individuals less than 60 and 35% for seniors over 60 (Goodwin et al. 2006). Hospitalization rates among seniors are highest followed by individuals in the 20–59 yr age group, and are lowest for individuals in the 6–19 yr age group. Mortality rates are highest among the 20–59 yr age group, followed by the 6–19 yr age group, and are lowest among seniors (60 yr and older). The age-specific contact rate matrix c_{ij} between age groups i and j is illustrated in the bottom panel of Fig. 1 and (9) in Appendix. The contact rate among individuals in the 6–12 yr age group is highest while the contact rate among the senior group is lowest (Edmunds et al. 1997; Mossong et al. 2008; Wallinga et al. 2006). All age-specific results are presented in terms of proportions of each age group, i.e., the number of individuals in each age group divided by the corresponding population size of each age group. The default values for the initial conditions and model parameters are given in Tables 1 and 2. Units are per day for all rates and baseline values are used throughout the manuscript unless otherwise indicated.

3.1 Optimal Age-Specific Vaccination Strategy

We evaluate the impact of optimal age-specific vaccination rates over the course of the influenza pandemic for $\mathcal{R}_0 = 1.8$ and a 30% vaccination coverage. Figure 2 compares a baseline situation (without vaccine) with an optimal vaccination strategy. Total vaccination coverage for this optimal vaccination strategy is 30% using the weight

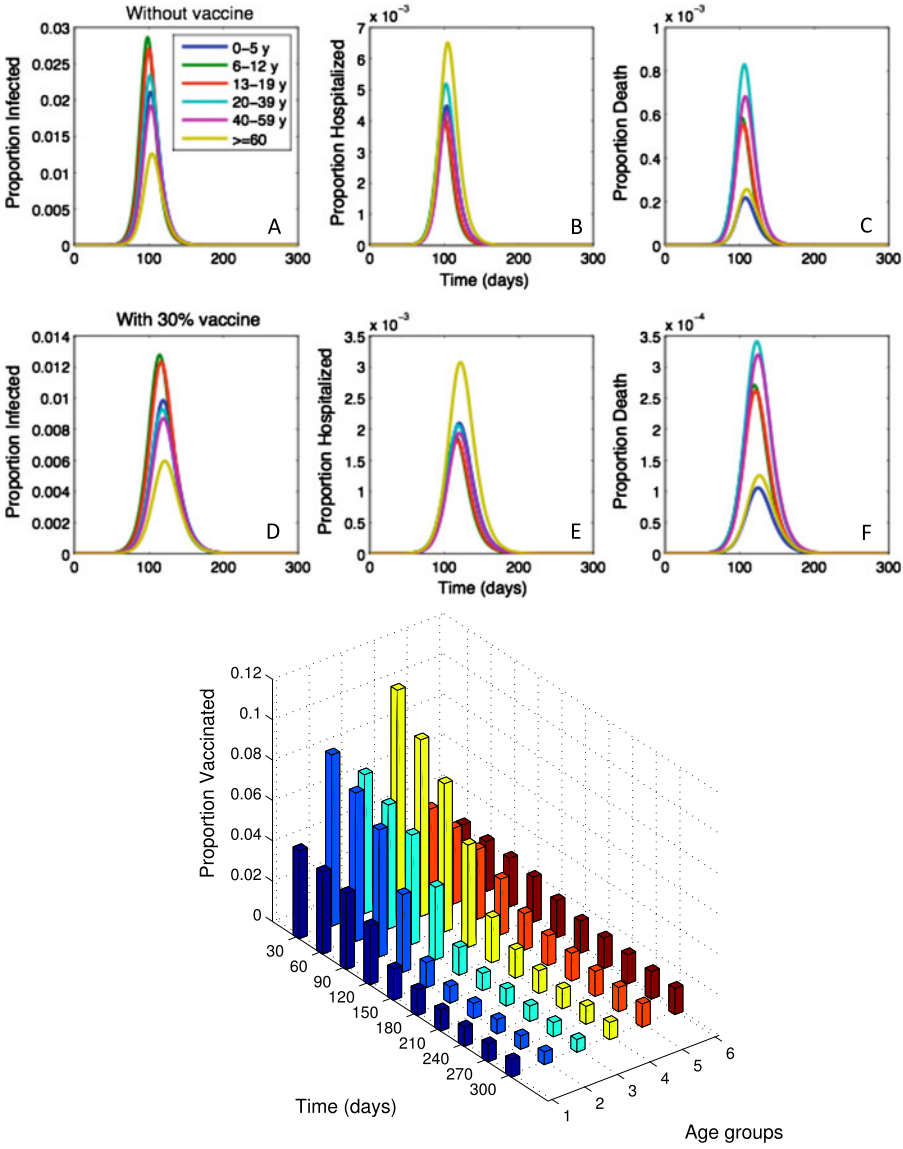

Fig. 2 (Color online) Age-specific incidence curves of infected, hospitalization and death proportions are displayed when $\mathcal{R}_0 = 1.8$. We compare a baseline situation where no vaccine is used (**A**)–(**C**) with results implementing optimal vaccination strategies (**D**)–(**F**). The time series of age-specific vaccinated proportion is shown for each age group (*bottom panel*)

constant of $W_i = 10^{15}$ for all i. Age-specific incidence curves of infected, hospitalized and dead proportions are shown in the absence of vaccine (Fig. 2A, B, C) and under vaccination (Fig. 2D, E, F). In the absence of vaccine, peak incidence (Fig. 2A) is reached near day 100 and the pandemic ends around day 150. In contrast, under the vaccination strategy, peak incidence is reached around day 120 and the pandemic

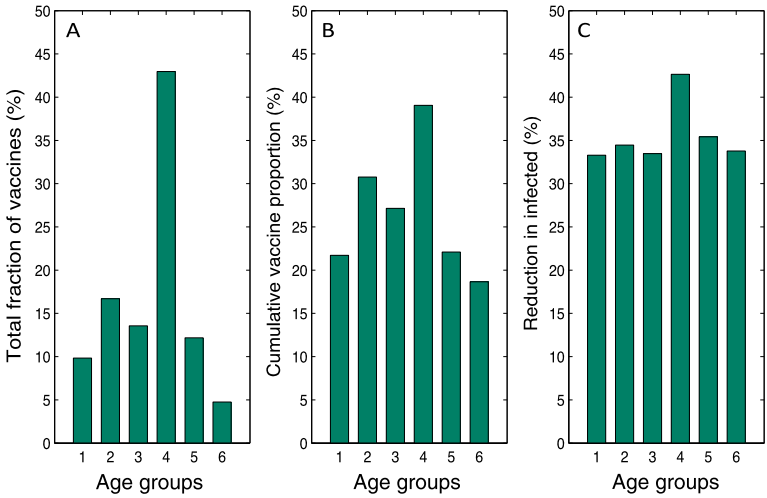

Fig. 3 Age-specific fractions of total vaccines and cumulative proportions of vaccinated are illustrated in (**A**) and (**B**), respectively, when $\mathcal{R}_0 = 1.8$. The percent age-specific reductions in infected classes are shown in (**C**) relative to the baseline (no vaccine) situation

ends around day 200 (Fig. 2D). The implementation of an optimal age-specific vaccination strategy yields reductions of approximately 50% in the peak size of infections, hospitalizations and deaths (Fig. 2D, E, F). Our results indicate that vaccination strategies generate longer pandemic durations while significantly reducing the pandemic peak size.

Time series of age-specific proportion of vaccinated individuals are displayed in the bottom panel of Fig. 2. All vaccination control functions are monotonically decreasing in time with the majority of control effort used during the first three months. The number of vaccinated individuals substantially decrease after 150 days (after 5 months when the incidence curves of infected start to decrease) for all age groups. Figure 2 (bottom panel) demonstrates that the proportions of vaccinated groups is largest in both the 20–39 yr age group and the 6–12 yr age group, while the senior age group obtains the smallest fraction of vaccinated individuals.

We explore the effectiveness of optimal age-specific vaccination on the cumulative number of infected individuals *relative* to the number of infected individuals in the absence of vaccination. Figure 3 shows the total fraction of vaccines allocated and the vaccination coverage by age group. The total fraction of vaccines represents the number of vaccinated individuals in each age group divided by the total number of vaccinated individuals (Fig. 3A). The results suggest that a substantially large fraction of the vaccine stockpile (about 43% of total vaccines) must be allocated to young adults (20–39 yr) while seniors should receive the smallest fraction of vaccines (about 5% of total vaccines available). Figure 3B shows the cumulative vaccination coverage by age group. Results suggest that the highest vaccination coverage (about 40%) must be achieved among the 20–39 yr age group.

The effectiveness of optimal age-specific vaccinations is also assessed by the reduction (%) in the cumulative number of infected individuals *relative* to the scenario

without interventions. The impact of optimal vaccinations in terms of reductions of infected individuals is shown in Fig. 3C. The reductions are almost uniform in all age groups (between 30 and 35%), with the exception of the 20–39 yr age group (around 43%). The implementation of optimal age-specific vaccinations yielded reductions of 36, 37, and 38% in the cumulative number of infected, hospitalized and dead individuals, respectively.

In this study, we considered the cost of vaccination to be the same regardless of the age group (Weight constant 1: W_i are the same for all i). However, the same vaccination coverage (30%) can be achieved by using different combinations of age-specific weight constants. We carried out a second case with different weight constants incorporating the cost of infection involving different risk levels such as age-specific mortality and hospitalization rates (Chowell et al. 2011). Therefore, smaller age-specific weight constants are used for the age groups 1, 5, and 6 due to a higher risk of infection (Weight constant 2: W_1, W_5, W_6 smaller than W_2, W_3, W_4). For this simulation, $R_0 = 1.8$ and vaccination coverage (VC) $= 30\%$ are used. Age-specific vaccinated proportions are increased in the age groups 1, 5, and 6, which reflects higher risk groups need to be more vaccinated. However, the results indicate that using Weight constant 2 yields very similar incidence curves and percent reductions in infected as when using Weight constant 1. The overall percent reduction among infected (36%) is essentially equal to the one using Weight constant 1.

3.2 Optimal Age-Specific Vaccination Strategies Under Different Vaccination Coverages

We study the effects of optimal vaccination strategies on the dynamics of influenza pandemics under different vaccination coverage levels when $\mathcal{R}_0 = 1.8$. Constraints on the availability of vaccine supplies were obtained by changing the effects of different weight constants on the controls. First, age-specific optimal vaccination controls under three different weight constants are compared in Fig. 4 using $W_i = 10^9$, 10^{12}, and 10^{15}. Under these weight constants, the overall vaccination coverages are 77%, 67%, and 30%, respectively. In the context of this study, larger values of W_i mean that the cost associated with vaccination is expensive; hence, less control is applied for larger W_i. For instance, a higher vaccination coverage (77%) is achieved using a relatively less expensive weight constant, $W_i = 10^9$, while a lower vaccination coverage (30%) is achieved by using a relatively more expensive weight constant $W_i = 10^{15}$. It is observed that the general shapes of control curves are similar (monotonic decreasing in time) with changes in magnitude for all age groups.

Figure 5 shows the impact of varying the weight constants in terms of the incidence of infected and vaccinated individuals. As weight constants are increased, cost of vaccination increases, resulting in an increase in the overall number of infected individuals and reductions in vaccination rates. This is due to the fact that large coverages of optimal age-specific vaccinations yield increased reductions in the overall number of infected individuals (Fig. 5G, H, I). A significant difference is observed in the magnitude of incidence curves for three classes (see the scale of the y-axis in Fig. 5G, H, I). From these results, it is observed that the use of early and sufficient implementation of vaccines (more than 67% vaccination coverage) contain an

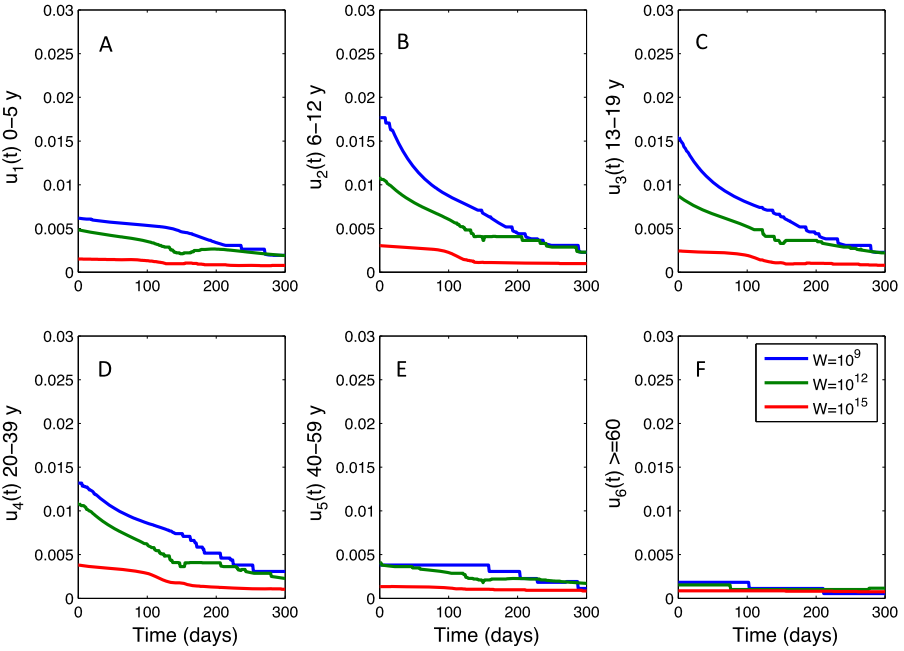

Fig. 4 (Color online) The impact of weight constants on age-specific vaccination rates are compared in (**A**)–(**F**) when $\mathcal{R}_0 = 1.8$ under three different weight constants $W = 10^9$, $W = 10^{12}$, and $W = 10^{15}$. Using these weight constants result in the range of vaccine coverages, 77, 67, 30%, respectively

influenza pandemic. In addition, our findings show shifts in the age-specific vaccination rates as the vaccination coverage decreases. For example, as the vaccine coverage decreases (with increase in weight constants, Fig. 5J, K, L), the proportion of vaccinated individuals among the 6–12 yr age group decreases while the proportion of the vaccinated individuals among the 20–39 yr age group increases. This result underscores a relationship between the age-prioritized vaccination strategies and vaccination coverage.

3.3 Optimal Age-Specific Vaccination Strategies Under Different Transmissibility Levels

The effects of optimal vaccination strategies as a function of $\mathcal{R}_0$ is presented in Fig. 6. For these simulations, the weight constant $W_i = 10^{15}$ is chosen to reflect realistic vaccination scenarios (i.e., when vaccine supplies are limited, less than 30%). The resulting vaccination coverages are 30%, 26%, and 21% for $\mathcal{R}_0 = 1.8$, $\mathcal{R}_0 = 2.4$, $\mathcal{R}_0 = 3.0$, respectively. Incidence curves of infected proportions for three different values of $\mathcal{R}_0$ are compared in Fig. 6(A)–(C). It can be observed that a larger $\mathcal{R}_0$ results in earlier pandemic peaks with larger pandemic sizes due to rapid spread of the pandemic. For instance, the pandemic peak at $\mathcal{R}_0 = 2.4$ (Fig. 6B) is twice the size of the pandemic peak for $\mathcal{R} = 1.8$ (Fig. 6A), while the pandemic peak for $\mathcal{R}_0 = 3.0$ (Fig. 6C) is twice the size of the pandemic peak for $\mathcal{R}_0 = 2.4$ (Fig. 6B). The

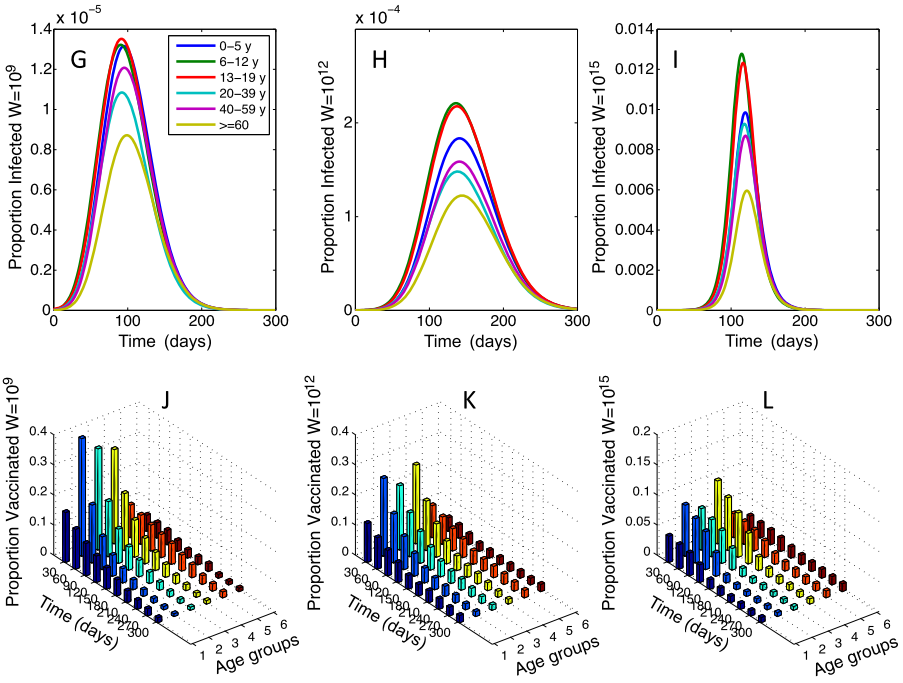

Fig. 5 (Color online) The impact of weight constants on age-specific incidence of infected and vaccinated proportions are explored when $\mathcal{R}_0 = 1.8$ under three different weight constants $W = 10^9$, $W = 10^{12}$, and $W = 10^{15}$. The corresponding age-specific incidence curves of infected proportions are illustrated in (**G**)–(**I**). Age-specific vaccinated proportions are displayed in (**J**)–(**L**). Overall vaccination coverages are 77%, 67% and 30% for $W = 10^9$, $W = 10^{12}$, and $W = 10^{15}$, respectively

pandemic ends around day 200, 120, and 100 for $\mathcal{R} = 1.8$, $\mathcal{R}_0 = 2.4$, $\mathcal{R}_0 = 3.0$, respectively. The time schedule of optimal vaccinated proportion is shown for each age group in Fig. 6 (D, E, F). Higher values of $\mathcal{R}_0$ (>=2.4) generates outbreaks that require the rapid implementation of optimal control policies with high vaccination coverage. As a result, high vaccination rates must be maintained for a short period of time since large $\mathcal{R}_0$'s quickly deplete the susceptible population (Fig. 6F). For the case when $\mathcal{R}_0 = 1.8$ (moderate level) and vaccination coverage is 30%, an optimal vaccination policy manages to reduce the magnitude of the influenza pandemic peak over a broader time window (Fig. 6D).

3.4 Cumulative Proportion of Vaccinated Individuals as Functions of Vaccination Coverage and $\mathcal{R}_0$

We also analyze the effects of different vaccination coverage levels and $\mathcal{R}_0$ on the cumulative number of vaccinated individuals. The cumulative proportion of vaccinated individuals for each age group is computed by determining the number of vaccinated individuals divided by the population size of each age group. Figure 7A presents the cumulative proportions of each age group under three different vaccination coverages, and denoted by VC = 77% ($W_i = 10^9$), VC = 67% ($W_i = 10^{12}$), and VC =

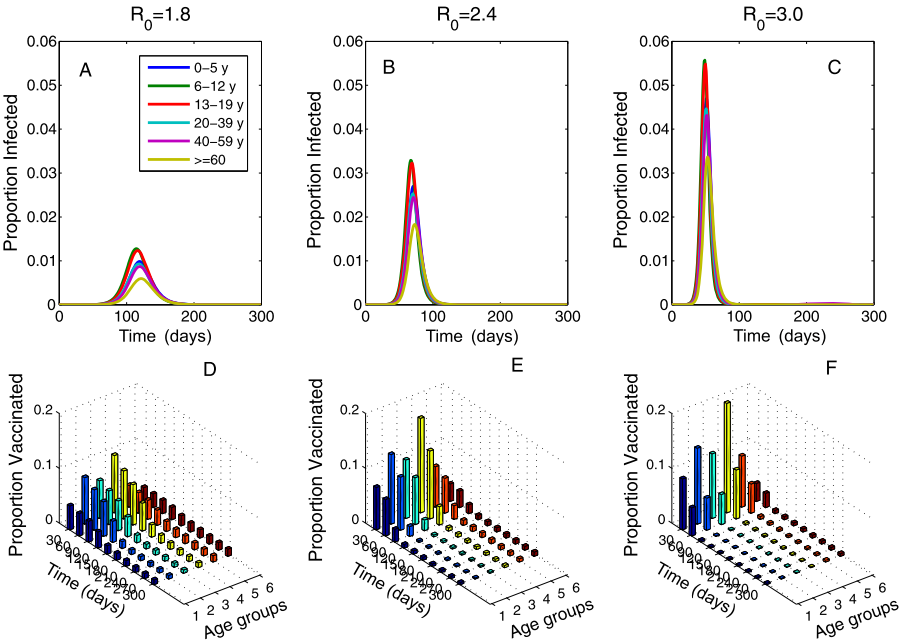

Fig. 6 (Color online) Age-specific incidence curves of infected proportions are plotted under three different $\mathcal{R}_0$ values: $\mathcal{R}_0 = 1.8$, $\mathcal{R}_0 = 2.4$, and $\mathcal{R}_0 = 3.0$ (**A**)–(**C**). Age-specific vaccinated proportions are plotted in the *bottom* panel (**D**)–(**F**). Total vaccination coverages are 30%, 26% and 21% for $\mathcal{R}_0 = 1.8$, $\mathcal{R}_0 = 2.4$, $\mathcal{R}_0 = 3.0$, respectively

Table 2 Age-specific baseline values used in numerical simulations

Age group	Population size	Hospitalization rates (days^{-1})	Mortality rates (days^{-1})	Vaccine efficacies (%)
0–5 yr	12933813	0.2135	0.0526	77.5
6–12 yr	15483929	0.1482	0.1491	77.5
13–19 yr	14253368	0.1482	0.1491	77.5
20–39 yr	31402356	0.2233	0.1704	77.5
40-59 yr	15735426	0.2233	0.1704	77.5
60>= yr	7277808	0.5165	0.0426	35

30% ($W_i = 10^{15}$) when $\mathcal{R}_0 = 1.8$. Overall profiles of age-specific proportions are similar as vaccine coverages decrease (or costs of vaccination increase). Not surprisingly, as the total vaccination coverage decreases, the overall cumulative proportion of vaccinated individuals decreases (Fig. 7A). Age groups with higher contact rates, namely, the 6–12 yr age group, require higher vaccination coverage when the total vaccine coverage is 77%. However, the 20–39 yr age group receives the highest vaccination coverage when the total vaccine coverage is less than 30%. The effectiveness of the optimal vaccination strategy is also assessed by comparing the reduction in the

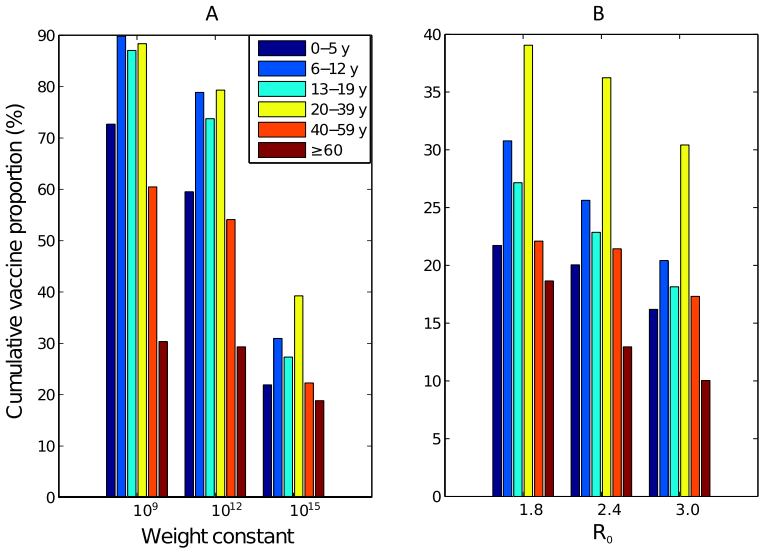

Fig. 7 (Color online) Cumulative proportions of vaccinated are compared under three different vaccination coverage levels when $\mathcal{R}_0 = 1.8$ in (**A**) ($W_i = 10^9$: VC = 77%, $W_i = 10^{12}$: VC = 67%, $W_i = 10^{15}$: VC = 30%). Cumulative proportions of vaccinated are displayed under three different $\mathcal{R}_0$ values in (**B**) ($\mathcal{R}_0 = 1.8$, $\mathcal{R}_0 = 2.4$, $\mathcal{R}_0 = 3.0$)

Table 3 Comparison of percent reductions in infected, hospitalized, and dead relative to the baseline scenario (no vaccine) under three different vaccine coverages when $\mathcal{R}_0 = 1.8$

	VC 77%	VC 67%	VC 30%
Infected	99%	97%	36%
Hospitalizations	99%	97%	37%
Deaths	99%	97%	38%

cumulative number of infected, hospitalized, and dead individuals *relative* to the ones in the absence of interventions. Table 3 shows relative reductions (%) under three different vaccination coverages. It shows higher reductions for higher vaccination coverages in all classes of infected, hospitalized, and dead. The use of VC = 77 or 67% generates significant reductions (99 or 97% in all classes of infected, hospitalized, and dead).

The impact of optimal vaccination strategies in terms of the cumulative proportion of vaccinated individuals as a function of $\mathcal{R}_0$ is presented in Fig. 7B, which compares the cumulative proportion of vaccinated individuals for three different values of $\mathcal{R}_0$ ($\mathcal{R}_0 = 1.8$, $\mathcal{R}_0 = 2.4$, and $\mathcal{R}_0 = 3$). For these simulations, the weight constant $W_i = 10^{15}$ is fixed, and the resulting vaccination coverages are 30%, 26%, and 21% for $\mathcal{R}_0 = 1.8$, $\mathcal{R}_0 = 2.4$, and $\mathcal{R}_0 = 3.0$, respectively. The overall proportion of vaccinated individuals decreases as $\mathcal{R}_0$ increases. Table 4 illustrates the reduction (%) as a function of $\mathcal{R}_0$. It shows high reductions for low $\mathcal{R}_0$ regardless of all classes (infected, hospitalized, and dead). All three classes show reductions of 35% or more when $\mathcal{R}_0 = 1.8$, however, as $\mathcal{R}_0$ increases, benefits decrease in all three classes.

Table 4 Comparison of percent reductions in infected, hospitalized, and dead with the baseline scenario (no vaccine) under three different $\mathcal{R}_0$

	$\mathcal{R}_0 = 1.8$ (VC 30%)	$\mathcal{R}_0 = 2.4$ (VC 26%)	$\mathcal{R}_0 = 3.0$ (VC 21%)
Infected	36%	24%	17%
Hospitalizations	37%	24%	16%
Deaths	38%	26%	18%

3.5 Optimal Age-Specific Vaccination Strategies Under a Time Delay of Vaccination

The timing of vaccine delivery or availability is always a critical issue in a pandemic vaccination plan. In the previous simulations, our model was based on an ideal setting (the vaccine is available at the beginning of a pandemic). There are several rationales behind this ideal setting: first, we assume that a universal vaccine will be available, which can be distributed at the onset of the pandemic. Second, a pandemic influenza always displays multiple waves (Miller et al. 2009). Under these scenarios, it is possible to achieve optimal vaccinations at the beginning of the second or third wave. Vaccination with the pandemic vaccine did not start until December 2009 in Mexico (Herrera-Valdez et al. 2011). That is, pandemic vaccination started 8 months after the onset of the novel virus. Therefore, we incorporated the time delay in our model by varying the time of the start of vaccination. The optimal control for each time delay case is recalculated under three different vaccination starting times; 30, 60, 90 days after the pandemic onset. The time delay effect is evaluated in terms of age-specific incidence curves of infected, age-specific vaccinated proportions, and the percent reductions of infected individuals relative to the baseline scenario. For all simulations, $R_0 = 1.8$ and vaccination coverage (VC) = 30% are used.

Figure 8 displays the age-specific incidence curves of infected and time series of vaccinated proportion under three different vaccination starting times. Delay of implementation of vaccination time leads to significant increases in the number of infected individuals for all age groups (left to right in top three Fig. 8). Also, a longer period of time delay, more intensive vaccination must be implemented in a shorter period of time (bottom three in Fig. 8). For all delay cases, the main targeted vaccinated group is the young adult group (20–39 yr). As the time delay increases, the proportion of vaccinated individuals among senior decreases dramatically while the proportion of the vaccinated individuals among the 0–5 yr age group increases. The implementation of delays of 30, 60, and 90 days yields the overall percent reductions of infected 35%, 27%, and 12%, respectively. Optimal vaccination strategy is still effective when they are applied at 30 days of the start of vaccination (35% reduction of infected). For the 90 days delay case, even though 30% vaccination coverage is put in place during the first month, only 12% percent reduction is obtained in the overall infected (Fig. 9).

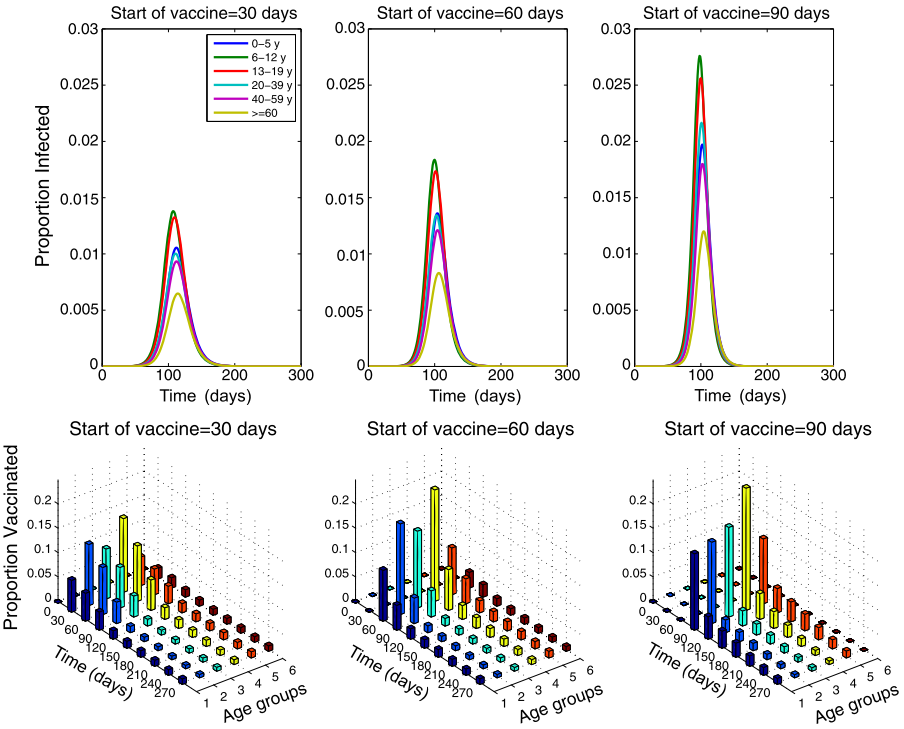

Fig. 8 (Color online) Age-specific incidence curves of infected are displayed under three different time of the start of vaccination (30, 60 and 90 days). The time series of age-specific vaccinated proportion is shown for each age group (*bottom panel*)

4 Discussion

The potential for a devastating influenza pandemic with high mortality and morbidity poses a serious challenge to public health systems around the world. As the 2009 H1N1 influenza pandemic has shown us, the lack of an "universal" influenza vaccine means that the availability of vaccines will be limited at best during early pandemic stages. In the absence of pharmaceutical tools, mitigation of disease spread relies on nonpharmaceutical interventions such as facial masks, social distancing, travel advisories, and isolation of infected individuals. The implementation of nonpharmaceutical measures could allow time for mass production of antiviral drugs and vaccines, enough to meet the needs of a large population (Ferguson et al. 2006; Gani et al. 2005; Fedson 2003; Germann et al. 2006; Lee et al. 2010; Nuno et al. 2007; Tracht et al. 2010). In addition to the mitigation of disease spread through nonpharmaceutical means, policy must also account for pharmacological measures to mitigate the effects of pandemic influenza. Under such global health emergencies posed by influenza pandemics, efficient prioritization of vaccine supplies or antivirals must be carefully assessed to mitigate the impact of severe pandemic outbreaks by considering various factors (e.g., population demographics, background

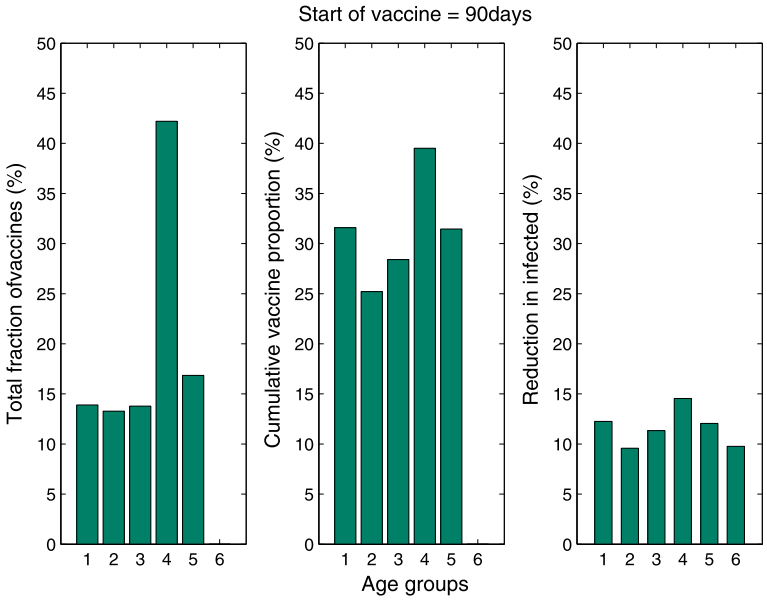

Fig. 9 Age-specific fractions of total vaccines and cumulative proportions of vaccinated are illustrated when the vaccine is delayed 90 days. The percent age-specific reductions in infected classes are shown relative to the baseline (no vaccine) situation

immunity levels, and resource availability Gostin and Berkman 2007; Kotalik 2005; Ulmer and Liu 2002).

In this study, we used a mathematical model of the transmission dynamics of pandemic influenza which accounted for age heterogeneity in disease transmissibility ($\mathcal{R}_0$), in addition to age-specific rates of infection, hospitalization and death (Chowell et al. 2009). Our mathematical framework incorporated time-dependent vaccination rates in the optimal control framework. Optimal vaccination policies were computed and analyzed under different vaccination coverage levels and the basic reproduction number ($\mathcal{R}_0$). While it is possible for mass vaccination to contain an influenza pandemic by bringing the susceptible population below the critical population size, under realistic scenarios (e.g., limited vaccine supplies), the optimal vaccination coverage for each group will differ. Our results demonstrate that the optimal age-specific vaccination rates vary with the total number of vaccine doses available. For example, for an overall vaccination coverage of 70%, the highest vaccination rate is allocated to 6–12 yr olds whereas the maximum vaccination rate is allocated to 20–39 yr for a lower vaccination coverage of 30% using a moderate value of $\mathcal{R}_0$ ($\mathcal{R}_0 = 1.8$). For higher $\mathcal{R}_0$ ($\mathcal{R}_0 >= 2.4$), we did not find qualitatively significant differences in age-specific vaccination rates (for all age groups) when vaccination coverage is $>70\%$. Our analysis confirmed that high contact rates due to the high level of activity among individuals within the school age group (6–12 yr) contributed the most to the overall transmissibility of influenza. Overall, the optimal vaccination strategy provided relatively high reductions of 30, 36, 37, and 38%, respectively, in the number of in-

fected, hospitalized and dead, respectively, when $\mathcal{R}_0 = 1.8$ and vaccination coverage of 30%.

Our findings also indicate that the duration of the vaccination period depends on $\mathcal{R}_0$. The earlier-maximum implementation of vaccination has always the greatest affect on the final size of infected individuals. Under a moderate range of $\mathcal{R}_0$ (greater than 1 but less than 2), our results show that the duration of vaccination should increase i.e. the duration of vaccination should be moderate over a longer time period (e.g., 4 or 5 months). For higher $\mathcal{R}_0$ ($\mathcal{R}_0 = 3.0$), a quick and substantial decrease in the pool of susceptibles would require the implementation of an intensive vaccination protocol within a shorter period of time (within 2 months of the onset of the pandemic). As transmissibility increases, we found that it is more efficient to vaccinate a larger portion of individuals in the 20–39 yr age group. Earlier vaccination is always the best strategy for controlling a pandemic outbreak for the ranges of $\mathcal{R}_0$ used in this study. For all ranges of $\mathcal{R}_0$, the vaccinated proportion for each age group does not appear to change with time when vaccination coverage is in the range of 20–30%. Under this scenario, maximal vaccination coverage occurred in the 20–39 yr age group, followed by the 6–12 yr age group, and the 13–19 yr age group. The vaccination coverage was lower among the 0–5 yr, 40–59 yr, and $>=60$ age groups. Our results show that as the vaccination delay increases, the young adult group (20–39 yr) and the age group (0–5 yr) must be vaccinated with substantial increases while the senior group (>60 yr) might get the minimum vaccine. Overall, the benefit of vaccination is significantly reduced as the time of the start of vaccination is delayed. In fact, mitigation is not possible if the timing of vaccination is too late (>120 days in this study).

The World Health Organization (WHO) prioritized a pandemic immunization plan which reflects the known epidemiology of influenza viruses, morbidity and mortality data, and vaccine efficacy to minimize the number of infection, hospitalization and dead, and to prevent the impact of negative socioeconomic effects that may result from an extreme global health scenario. Many developed countries can provide enough vaccine supplies to immunize a substantial fraction of their populations while the availability of vaccines to individuals in developing countries in the midst of a pandemic outbreak remains limited. Hence, it becomes important not only to establish increased global production of these resources to many countries but also to effectively allocate this key resource. Future studies of this type should account for asymptomatic cases, other risk factors (e.g., high-risk subpopulations) and constraints imposed by current vaccine technologies on delays from pandemic onset to the start of vaccination campaigns.

Our results highlight the potential impact of pre-pandemic immunization with pandemic-type viruses before a pandemic hits. However, more research on the vaccine efficacy and safety and long-term effects of this strategy on public health is needed (Stohr 2010). The work presented here should improve our understanding of age-specific optimal vaccination policies on reducing rates of infection, hospitalization and dead among different age groups with different levels of activity and demographics. We believe that an improved understanding of optimal vaccination protocols will provide policymakers with the information needed to plan effective strategies for mitigating the effects of influenza pandemics in real time. In addition,

these types of strategies will allow countries to respond to the needs of high-priority populations, which could reduce the health and economic impact of A (H1N1). Ultimately, the identification of optimal vaccine distributions in different age groups as a function of time may provide necessary information for the development and evaluation of vaccine delivery strategies in the presence of limited resources.

Appendix

The goal is to minimize the number of infectious individuals over a finite time interval $[0, T]$ at a minimal cost of vaccination efforts during the course of a single influenza pandemic outbreak. The objective functional $\mathcal{F}$ is defined in (2). The optimal control problem is to find an optimal pairs, $(U^*(t), X^*(t))$ such that

$$\mathcal{F}\big(U^*(t)\big) = \min_{\Omega} \mathcal{F}\big(U(t)\big) \tag{4}$$

where $\Omega = \{U(t) \in L^2(0,T)^6 \| a \le u_i(t) \le b, i = 1, \ldots, 6, t \in [0,T]\}$ subject to the state equations given by model (1). Given the criterion (2) and the regularity of the system of equations (1), the existence of optimal controls is guaranteed by standard results in control theory (Fleming and Rishel 1975). The necessary conditions of optimal solutions are derived from Pontryagin's Maximum Principle (Pontryagin et al. 1962). This principle converts the system (1)–(3) into the problem of minimizing the Hamiltonian H given by

$$\begin{aligned}
H = &\sum_{i=1}^{6}\left[I_i(t) + \frac{W_i}{2}u_i^2(t)\right] \\
&+ \sum_{i=1}^{6}\lambda_{S_i}(t)\left\{-u_i(t)S_i(t) - \sum_{i=1}^{6}\beta_{ij}\frac{(I_j(t)+J_j(t))}{N(t)}S_i(t)\right\} \\
&+ \sum_{i=1}^{6}\lambda_{V_i}(t)\left\{\epsilon_i u_i(t)S_i(t) - \eta V_i(t) - \sum_{i=1}^{6}\beta_{ij}\frac{(I_j(t)+J_j(t))}{N(t)}V_i(t)\right\} \\
&+ \sum_{i=1}^{6}\lambda_{F_i}(t)\left\{(1-\epsilon_i)u_i(t)S_i(t) - \sum_{i=1}^{6}\beta_{ij}\frac{(I_j(t)+J_j(t))}{N(t)}F_i(t)\right\} \\
&+ \sum_{i=1}^{6}\lambda_{E_i}(t)\left\{\sum_{i=1}^{6}\beta_{ij}\frac{(I_j(t)+J_j(t))}{N(t)}\big(S_i(t)+V_i(t)+F_i(t)\big) - kE_i(t)\right\} \\
&+ \sum_{i=1}^{6}\lambda_{I_i}(t)\big\{kE_i(t) - (\alpha_i+\gamma_1)I_i(t)\big\} \\
&+ \sum_{i=1}^{6}\lambda_{J_i}(t)\big\{\alpha_i I_i(t) - (\gamma_2+\delta_i)J_i(t)\big\}
\end{aligned} \tag{5}$$

From this Hamiltonian and Pontryagin's maximum principle (Pontryagin et al. 1962), we obtain the following theorem.

Theorem 1 *There exist optimal controls $U^*(t)$ and corresponding solutions $X^*(t)$ that minimize $\mathcal{F}(U)$ over Ω. In order for the above statement to be true, it is necessary that there exist continuous functions $\Lambda_i(t)$ such that*

$$\begin{aligned}
\dot{\lambda}_{S_i}(t) &= \left\{u_i(t) + \sum_{i=1}^{6} \beta_{ij} \frac{(I_j(t) + J_j(t))}{N(t)}\right\}\lambda_{S_i}(t) - \epsilon_i u_i(t)\lambda_{V_i}(t) \\
&\quad - (1-\epsilon_i)u_i(t)\lambda_{F_i}(t) - \sum_{i=1}^{6} \beta_{ij} \frac{(I_j(t) + J_j(t))}{N(t)}\lambda_{E_i}(t) \\
\dot{\lambda}_{V_i}(t) &= \left\{\eta + \sum_{i=1}^{6} \beta_{ij} \frac{(I_j(t) + J_j(t))}{N(t)}\right\}\lambda_{V_i}(t) - \sum_{i=1}^{6} \beta_{ij} \frac{(I_j(t) + J_j(t))}{N(t)}\lambda_{E_i}(t) \\
\dot{\lambda}_{F_i}(t) &= \sum_{i=1}^{6} \beta_{ij} \frac{(I_j(t) + J_j(t))}{N(t)}\lambda_{F_i}(t) - \sum_{i=1}^{6} \beta_{ij} \frac{(I_j(t) + J_j(t))}{N(t)}\lambda_{E_i}(t) \\
\dot{\lambda}_{E_i}(t) &= k\lambda_{E_i}(t) - k\lambda_{I_i}(t) \\
\dot{\lambda}_{I_i}(t) &= -1 + \sum_{j=1}^{6} \frac{\beta_{ji}}{N(t)}\big\{S_j(t)\big(\lambda_{S_j}(t) - \lambda_{E_j}(t)\big) + V_j(t)\big(\lambda_{V_j}(t) - \lambda_{E_j}(t)\big) \\
&\quad + F_j(t)\big(\lambda_{F_j}(t) - \lambda_{E_j}(t)\big)\big\} + (\alpha_i + \gamma_1)\lambda_{I_i}(t) - \alpha_i\lambda_{J_i}(t), \\
\dot{\lambda}_{J_i}(t) &= \sum_{j=1}^{6} \frac{\beta_{ji}}{N(t)}\big\{S_j(t)\big(\lambda_{S_j}(t) - \lambda_{E_j}(t)\big) + V_j(t)\big(\lambda_{V_j}(t) - \lambda_{E_j}(t)\big) \\
&\quad + F_j(t)\big(\lambda_{F_j}(t) - \lambda_{E_j}(t)\big)\big\} + (\gamma_2 + \delta_i)\lambda_{J_i}(t),
\end{aligned} \tag{6}$$

with the transversality conditions,

$$\Lambda_i(T) = 0, \quad i = 1, \ldots, 6 \tag{7}$$

where $\Lambda_i(t) = (\lambda_{S_i}, \lambda_{V_i}, \lambda_{F_i}, \lambda_{E_i}, \lambda_{I_i}, \lambda_{J_i})$ and furthermore,

$$u_i^*(t) = \min\left\{\max\left\{a, \frac{S_i(t)}{W_i}\big[\lambda_{S_i}(t) - \epsilon_i\lambda_{V_i}(t) - (1-\epsilon_i)\lambda_{F_i}(t)\big]\right\}, b\right\}. \tag{8}$$

Proof The existence of optimal controls follows from Corollary 4.1 of Fleming and Rishel (1975) since the integrand of $\mathcal{F}$ is a convex function of $U(t)$ and the state system satisfies the *Lipschitz* property with respect to the state variables. The following can be derived from the Pontryagin's maximum principle (Pontryagin et al. 1962):

$$\frac{d\lambda_{S_i}(t)}{dt} = -\frac{\partial H}{\partial S_i}, \qquad \frac{d\lambda_{V_i}(t)}{dt} = -\frac{\partial H}{\partial V_i}, \qquad \frac{d\lambda_{F_i}(t)}{dt} = -\frac{\partial H}{\partial F_i},$$

$$\frac{d\lambda_{E_i}(t)}{dt} = -\frac{\partial H}{\partial E_i}, \qquad \frac{d\lambda_{I_i}(t)}{dt} = -\frac{\partial H}{\partial I_i}, \qquad \frac{d\lambda_{J_i}(t)}{dt} = -\frac{\partial H}{\partial J_i},$$

with $\Lambda_i(T) = 0$ for $i = 1, \ldots, 6$ and evaluated at the optimal controls and corresponding states, which results in the adjoint system (6). The Hamiltonian H is minimized with respect to the controls, so we differentiate H with respect to u_i on the set Ω, respectively, giving the following optimality conditions:

$$\frac{\partial H}{\partial u_i} = W_i u_i(t) - \lambda_{S_i}(t) S_i(t) + \epsilon_i \lambda_{V_i}(t) S_i(t) + (1-\epsilon_i)\lambda_{F_i}(t) S_i(t) = 0$$
$$\text{at } u_i(t) = u_i^*(t).$$

Solving for $u_i^*(t)$, we obtain

$$u_i^*(t) = \frac{S_i(t)}{W_i}\big[\lambda_{S_i}(t) - \epsilon_i \lambda_{V_i}(t) - (1-\epsilon_i)\lambda_{F_i}(t)\big].$$

By using the standard argument for bounds $a \le u_i(t) \le b$, we have the properties (8).

$$(c_{ij}) = \begin{pmatrix} 169.14 & 31.47 & 17.76 & 34.50 & 15.83 & 11.47 \\ 31.47 & 274.51 & 32.31 & 34.86 & 20.61 & 11.50 \\ 17.76 & 32.31 & 224.25 & 50.75 & 37.52 & 14.96 \\ 34.50 & 34.86 & 50.75 & 75.66 & 49.45 & 25.08 \\ 15.83 & 20.61 & 37.52 & 49.45 & 61.26 & 32.99 \\ 11.47 & 11.50 & 14.96 & 25.08 & 32.99 & 54.23 \end{pmatrix} \tag{9}$$

The contact rate matrix, (c_{ij}), represents the mixing rates between age groups i and j per week with higher rates within each age group (when $i = j$) than between age groups when $i \neq j$. □

References

Aaby, K., Abbey, R., Herrmann, J., Treadwell, M., Jordan, C., & Wood, K. (2006). Embracing computer modeling to address pandemic influenza in the 21st century. *J. Public Health Manag. Pract.*, *12*(4), 365–372.

Behncke, H. (2000). Optimal control of deterministic pandemics. *Optim. Control Appl. Methods*, *21*, 269–285.

Blayneh, K., Cao, Y., & Kwon, H. (2009). Optimal control of vector-borne disease: treatment and prevention. *Discrete Contin. Dyn. Syst., Ser. B*, *11*(3), 587–611.

Centers For Disease Control and Prevention (2009). Large-scale vaccination clinic output and staffing estimates: An example. www.cdc.gov/h1n1flu/vaccination/pdf/A-Wortley-H1N1-sample-clinic.pdf.

Cho, B., Hicks, K., Honeycutt, A., Hupert, N., Khavjou, O., Messonnier, M., & Washington, M. (2011). A tool for the economic analysis of mass prophylaxis operations with an application to H1N1 influenza vaccination clinics. *J. Public Health Manag. Pract.*, *17*, E22–E28.

Chowell, G., Miller, M. A., & Viboud, C. (2008). Seasonal influenza in the United States, France and Australia: transmission and prospects for control. *Epidemiol. Infect.*, *136*, 852–864.

Chowell, G., Viboud, C., Wang, X., Bertozzi, S., & Miller, M. (2009). Adaptive vaccination strategies to mitigate pandemic influenza: Mexico as a case study. *PLoS ONE*, *12*, e8164.

Chowell, G., Bertozzi, S. M., Colchero, M. A., Lopez-Gatell, H., Alpuche-Aranda, C., Hernandez, M., & Miller, M. A. (2009). Severe respiratory disease concurrent with the circulation of H1N1 influenza. *N. Engl. J. Med.*, *361*, 674–679.

Chowell, G., Echevarría-Zuno, S., Viboud, C., Simonsen, L., Tamerius, J., Miller, M. A., & Borja-Aburto, V. (2011). Characterizing the epidemiology of the 2009 influenza A/H1N1 pandemic in Mexico. *PLoS Med.*, *8*(5), e1000436.

Edmunds, W. J., O'Callaghan, C. J., & Nokes, D. J. (1997). Who mixes with whom? A method to determine the contact patterns of adults that may lead to the spread of airborne infections. *Proc. Biol. Sci.*, *264*(1384), 949–957.

Ferguson, N. M., Cummings, D. T., Fraser, C., Cajka, J. C., Cooley, P. C., & Burke, D. S. (2006). Strategies for mitigating an influenza pandemic. *Nature*, *442*(7101), 448–452.

Fleming, W. H., & Rishel, R. W. (1975). *Deterministic and stochastic optimal control*. New York: Springer.

Gani, R., Hughes, H., Fleming, D., Grifin, T., Medlock, J., & Leach, S. (2005). Potential impact of antiviral use during influenza pandemic. *Emerg. Infect. Dis.*, *11*, 1355–1362.

Fedson, D. S. (2003). Pandemic influenza and the global vaccine supply. *Clin. Infect. Dis.*, *36*(12), 1562–1563.

Germann, T. C., Kadau, K., Longini, I. M., & Macken, C. A. (2006). Mitigation strategies for pandemic influenza in the United States. *Proc. Natl. Acad. Sci. USA*, *103*(15), 5935–5940.

Goodwin, K., Viboud, C., & Simonsen, L. (2006). Antibody response to influenza vaccination in the elderly: a quantitative review. *Vaccine*, *24*(8), 1159–1169.

Gostin, L., & Berkman, B. (2007). Pandemic influenza: ethics, law, and the public's health. *Adm. Law Rev.*, *59*(1), 121–175.

http://www.phac-aspc.gc.ca/alert-alerte/h1n1/vacc/vacc-archive/dist-archive-eng.php Public Health Agency of Canada (2010).

http://www.cdc.gov/mmwr/preview/mmwrhtml/mm5912a2.htm CDC (2010).

Hansen, E., & Day, T. Optimal control of pandemics with limited resources J. Math. Biol. doi:10.1007/s00285-010-0341-0.

Herrera-Valdez, M., Cruz-Aponte, M., & Castillo-Chavez, C. (2011). Multiple outbreaks for the same pandemic: local transportation and social distancing explain the different "waves" of A-H1N1pdm cases observed in Mexico during 2009. *Math. Biosci. Eng.*, *8*, 21–48.

Health Industry Distributors Association: 2008–2009 influenza vaccine production and distribution 2009 [www.flusupplynews.com/documents/09 FluBrief 000.pdf].

Hill, A. N., & Longini, I. M. Jr. (2003). The critical vaccination fraction for heterogeneous pandemic models. *Math. Biosci.*, *181*(1), 85–106.

Jung, E., Lenhart, S., & Feng, Z. (2002). Optimal control of treatments in a two strain tuberculosis model. *Discrete Contin. Dyn. Syst., Ser. B*, *2*, 473–482.

Knipl, D. H., & Rost, G. (2011). Modelling the strategies for age specific vaccination scheduling during influenza pandemic outbreaks. *Math. Biosci. Eng.*, *8*(1), 123–139.

Kotalik, J. (2005). Preparing for an influenza pandemic: ethical issues. *Bioethics*, *19*(4), 422–431.

Lee, S., Chowell, G., & Castillo-Chavez, C. (2010). Optimal control of influenza pandemics: the role of antiviral treatment and isolation. *J. Theor. Biol.*, *265*, 136–150.

Lee, S., Morales, R., & Castillo-Chavez, C. (2011). A note on the use of influenza vaccination strategies when supply is limited. *Math. Biosci. Eng.*, *8*(1), 171–182.

Lenhart, S., & Workman, J. T. (2007). *Optimal control applied to biological models*. *CRC Mathematical and Computational Biology series*. London: Chapman & Hall.

Libenson, F. Llegaron al Edomex 66 mil Vacunas Contra AH1N1 (2009). http://elinformantemexico.com/index.php/noticias/llegaron-al-edomex-66-mil-vacunascontra-ah1n1-franklin-libenson-violante.html.

Lipsitch, M., Riley, S., Cauchemez, S., Ghani, A. C., & Ferguson, N. M. (2009). Managing and reducing uncertainty in an emerging influenza pandemic. *N. Engl. J. Med.*, *361*, 112–115.

Macroepidemiology of Influenza Vaccination Study Group (2005). The Macro-epidemiology of influenza vaccination in 56 countries, 1997–2003. *Vaccine*, *23*(44), 5133–5143.

Merler, S., Ajelli, M., & Rizzo, C. (2009). Age-prioritized use of antivirals during an influenza pandemic. *BMC Infect. Dis.*, *9*, 117. doi:10.1186/1471-2334-9-117.

Medlock, J., Meyers, L. A., & Galvani, A. (2009). Optimizing allocation for a delayed influenza vaccination campaign PLoS Curr Influenza RRN1134.

Miller, M., Viboud, C., Balinska, M., & Simonsen, L. (2009). The signature features of influenza pandemics—implications for policy. *N. Engl. J. Med.*, *360*(25), 2595–2598.

Mossong, J., et al. (2008). Social contacts and mixing patterns relevant to the spread of infectious diseases. *PLoS Med.*, *5*(3), e74.

Mylius, S. D., et al. (2008). Optimal allocation of pandemic influenza vaccine depends on age, risk and timing. *Vaccine*, *26*(29–30), 3742–3749.

Nishiura, H., Castillo-Chavez, C., Safan, M., & Chowell, G. (2009). Transmission potential of the new influenza (h1N1) virus and its age-specificity in Japan. *Euro Surveill.*, *14*(22), 1–4.

Nuno, M., Chowell, G., & Gumel, A. B. (2007). Assessing the role of basic control measures, antivirals and vaccine in curtailing pandemic influenza: scenarios for the US, UK and the Netherlands. *J. R. Soc. Interface*, *224*(14), 505–521.

Oliver Wyman Group and Program for Appropriate Technology in Health: Influenza vaccine strategies for broad global access, key findings and project methodology (2007). www.path.org/files/VAC_infl_publ_rpt_10-07.pdf.

Oshitani, H., Kamigaki, T., & Suzuki, A. (2008). Major issues and challenges of influenza pandemic preparedness in developing countries. *Emerg. Infect. Dis.*, *14*(6), 875–880.

Patel, R., Longini, I. M. Jr., & Halloran, M. E. (2005). Finding optimal vaccination strategies for pandemic influenza using genetic algorithms. *J. Theor. Biol.*, *234*(2), 201–212.

Peterborough County-city health unit pandemic influenza plan, Annex A: Mass vaccination plan (2010). http://pcchu.peterborough.on.ca/IC/IC-pandemic-plan.html.

Phillips, F., & Williamson, J. (2005). Local health department applies incident management system for successful mass influenza clinics. *J. Public Health Manag. Pract.*, *11*(4), 269.

Pontryagin, L. S., Boltyanskii, V. G., Gamkrelidze, R. V., & Mishchenko, E. F. (1962). *The mathematical theory of optimal processes*. New Jersey: Wiley.

Rowthorn, R. E., Laxminarayan, R., & Gilligan, C. A. (2009). Optimal control of pandemics in metapopulations. *Proc. R. Soc.* doi:10.1098/?rsif.2008.0402.

Stohr, K. (2010). Vaccinate before the next pandemic? *Nature*, *465*, 13.

Tennenbaum, S. (2008). Simple criteria for finding (nearly) optimal vaccination strategies. *J. Theor. Biol.*, *250*(4), 673–683.

Tracht, S. M., Del Valle, S. Y., & Hyman, J. M. (2010). Mathematical modeling of the effectiveness of facemasks in reducing the spread of novel influenza A (H1N1). *PLoS ONE*, *105*(2), e9018.

Tuite, A. R., Fisman, D. N., Kwong, J. C., & Greer, A. L. (2010). Optimal pandemic influenza vaccine allocation strategies for the Canadian population. *PLoS ONE*, *5*(5), e10520. doi:10.1371/journal.pone.0010520.

Ulmer, J., & Liu, M. (2002). Ethical issues for vaccines and immunization. *Nat. Rev. Immunol.*, *2*, 291–296.

Valadez, B. Aplicadas, Solo 10% de las Dosis Contra el A/H1N1 (2010). http://www.milenio.com/node/368812.

Wallinga, J., Teunis, P., & Kretzschmar, M. (2006). Using data on social contacts to estimate age-specific transmission parameters for respiratory-spread infectious agents. *Am. J. Epidemiol.*, *164*(10), 936–944.

Washington, M. (2009). Evaluating the capability and cost of a mass influenza and pneumococcal vaccination clinic via computer simulation. *Med. Decis. Mak.*, *29*(4), 414–423.